The Astrophysical Journal Letters, 894:L3 (11pp), 2020 May 1 https://doi.org/10.3847/2041-8213/ab8ad9

Near-infrared Methanol Bands Probe Energetic Processing of Icy Outer Solar System Objects

Riccardo Giovanni Urso[1], Donia Baklouti[1], Zahia Djouadi[1], Noemí Pinilla-Alonso[2], and Rosario Brunetto[1]
[1] Université Paris-Saclay, CNRS, Institut d'astrophysique spatiale, F-91405, Orsay, France; rurso@ias.u-psud.fr
[2] Florida Space Institute, University of Central Florida, Orlando, FL, USA
Received 2020 March 6; revised 2020 April 17; accepted 2020 April 17; published 2020 April 29

Abstract

Frozen methanol was detected in the outer solar system on the surfaces of the Centaur 5145 Pholus, the Trans-Neptunian Object (55638) 2002 VE_{95}, and more recently on (486958) Arrokoth. The icy surfaces of these objects are subjected to solar and cosmic ions that modify the physico-chemical properties of their surface. To study the effects of ion bombardment on methanol-rich surfaces, we performed experiments of ion irradiation of H_2O:CH_3OH mixtures and we monitored the evolution of the methanol near-infrared bands. We observed significant variations of the 2.34/2.27 μm methanol band ratios as a function of the irradiation dose. We then used the Arrokoth and Pholus spectra to test the 2.34/2.27 μm band ratio as a probe of irradiation of methanol-rich surfaces, and we estimated the timescales of processing by solar and cosmic ions. Our results indicate that solar energetic particles are the main drivers of changes in the near-infrared spectra of frozen surfaces in the outer solar system.

Unified Astronomy Thesaurus concepts: Laboratory astrophysics (2004); Small solar system bodies (1469); Surface composition (2115); Surface processes (2116); Solar energetic particles (1491); Cosmochemistry (331); Spectroscopy (1558)

1. Introduction

Methanol is one of the most abundant molecules in the solid phase of the interstellar medium (e.g., Boogert et al. 2015). Methanol is also present in the solar system: detected in comets (e.g., Geiss et al. 1991; Eberhardt et al. 1994; Altwegg et al. 2017), and at the surfaces of the centaur 5145 Pholus (Cruikshank et al. 1998), the trans-Neptunian object 55638 2002 VE_{95} (Barucci et al. 2006), and the small Kuiper-belt object (KBO) (486958) Arrokoth, a target of the New Horizons extended mission (Stern et al. 2019; Grundy et al. 2020). Arrokoth is a cold classical KBO, and it is expected to preserve information on the physico-chemical properties of the outer solar cloud (e.g., Nesvorný 2018; Souza-Feliciano et al. 2018; McKinnon et al. 2020).

The three noncometary objects mentioned above show red spectral slopes in the visible and near-infrared (vis-NIR). The composition, origin, and evolution of these ultra-red objects are still under debate. Dalle Ore et al. (2011) suggested two leading hypotheses to explain the red color. The *nature* hypothesis refers to the possibility that red materials were inherited from the presolar cloud or were accreted in the protoplanetary disk; the *nurture* hypothesis attributes the presence of red materials to post-accretional processing by solar and cosmic ions. In fact, atmosphere-less surfaces undergo energetic processing (EP) due to interactions with solar wind (SW) ions with energies of $\sim$1 keV/u, solar energetic particles (SEP) with energies between tens of keV/u and hundreds of MeV/u, cosmic rays (CR) with energies between tens of keV and 10^{18} keV (e.g., Johnson 1990; Strazzulla et al. 2003; Mewaldt et al. 2007; Rothard et al. 2017), and UV photons.

Laboratory experiments studying the EP of methanol-rich ices have shown the formation of various compounds (e.g., Rothard et al. 2017, and references therein for details on the physico-chemical process). Among the by-products of methanol irradiation, CO, H_2CO, CH_4, C_2H_6, and other species of prebiotic interest were detected (e.g., Allamandola et al. 1988; Gerakines et al. 1996; Palumbo et al. 1999; Hudson & Moore 2000; Bennett et al. 2007; de Barros et al. 2011; Modica et al. 2012; Chen et al. 2013; Chuang et al. 2017; Nuevo et al. 2018). Furthermore, the initially flat and bright vis-NIR spectrum of frozen methanol displayed a red slope upon bombardment with 10–400 keV ions or electrons (Brunetto et al. 2006; Poston et al. 2018). EP may be occurring at the surface of icy objects and contribute to their red color. However, because vis-NIR slopes are sensitive to the physical structure of materials, such as porosity and roughness (e.g., Hapke 2012), information about EP of surfaces cannot be unambiguously obtained from these slopes.

So far, the presence of methanol in frozen objects has been revealed through its main NIR band at 2.27 μm (4400 cm^{-1}), i.e., the combination of C–H asymmetric stretching and deformation modes. Methanol shows another band at 2.34 μm (4280 cm^{-1}), i.e., the combination of C–H symmetric stretching and deformation modes (Cruikshank et al. 1998), and laboratory experiments have revealed that this feature was more sensitive to ion bombardment than the 2.27 μm band (Brunetto et al. 2005). In this work we provide information on the extent of processing experienced by methanol-rich surfaces by exploiting the different sensitivities of the two methanol bands to ion bombardment and studying the evolution of the 2.34/2.27 μm methanol band ratio (hereafter, 2.34/2.27 ratio) upon irradiation.

2. Methods

We performed reflectance and transmittance IR spectroscopy on CH_3OH:H_2O = 5:1 and CH_3OH:H_2O = 1:1 mixtures bombarded with 40 keV H^+. The resulting spectra were compared to the spectra of Arrokoth and Pholus. Mixture ratios and irradiation temperatures were chosen to simulate surfaces with different water and methanol relative abundances

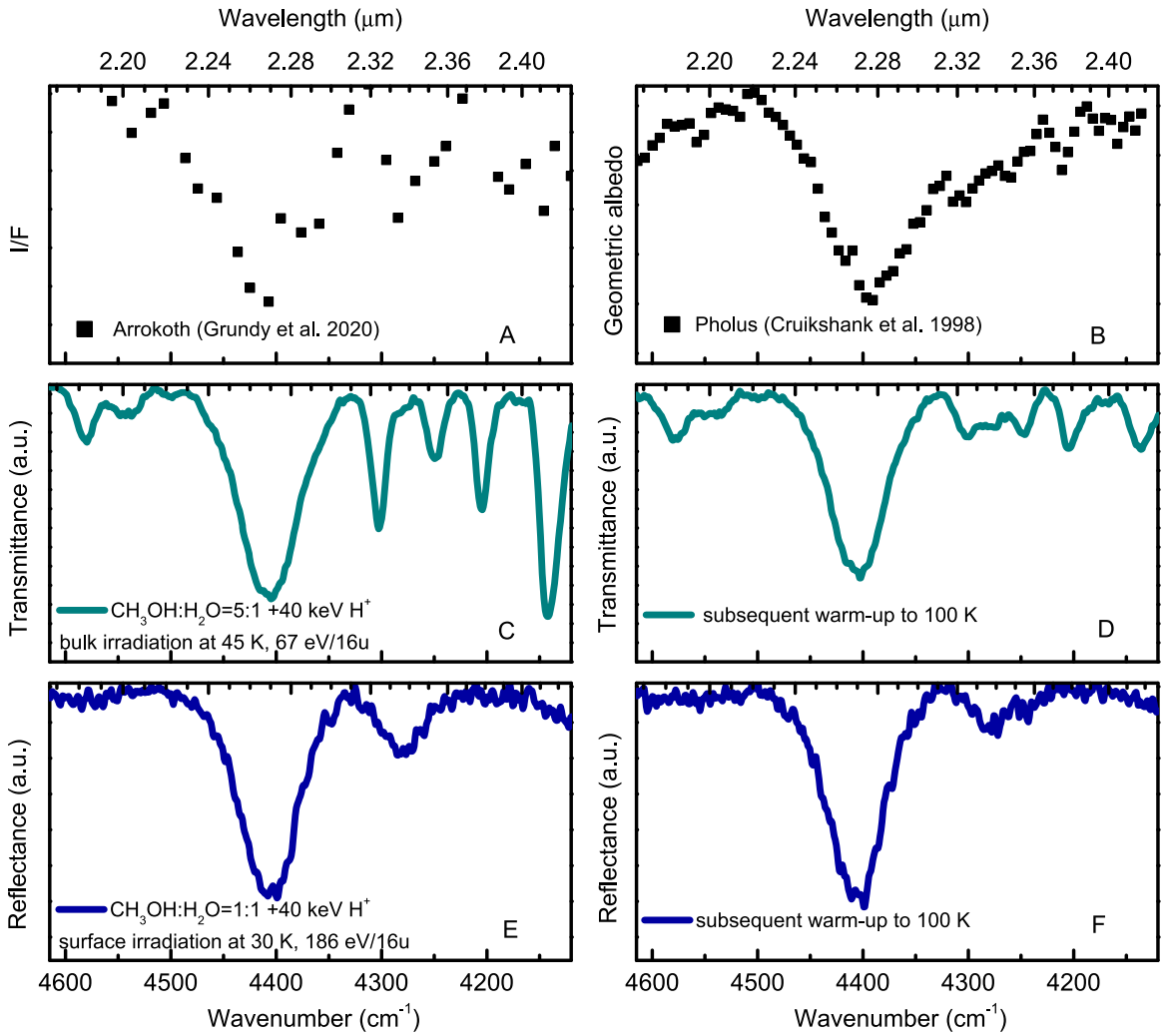

Figure 1. Arrokoth (panel (A)), Pholus (panel (B)), and laboratory spectra of CH_3OH:H_2O mixtures bombarded with 40 keV H^+. Transmittance spectra acquired on a fully irradiated ice (panels (C) and (D)); reflectance spectra acquired on an ice irradiated on the first micron (panels (E) and (F)).

and to be as close as possible to the temperatures estimated on methanol-rich bodies (i.e., 30–100 K Cruikshank et al. 1998; Stern et al. 2019; Grundy et al. 2020).

Experiments were performed with the IrradiatioN de Glaces et Météorites Analysées par Réflectance vis-IR (INGMAR, Lantz et al. 2017) setup at IAS-CSNSM (Orsay, France). CH_3OH and H_2O were injected into a vacuum chamber ($P \sim 5 \times 10^{-8}$ mbar) where they condensed on a substrate in thermal contact with a closed-cycle He-cryocooler (temperature $\geqslant$15 K). After deposition, frozen mixtures were warmed up to 30 or 45 K and then bombarded with 40 keV H^+ produced by the SIDONIE ion accelerator (CSNSM, Orsay; Chauvin et al. 2004). In this work the dose, i.e., energy deposited per unit volume in the sample by incident radiation, is given in eV/16u, where u is the unified atomic mass unit (e.g., Strazzulla & Johnson 1991). After irradiation, samples were warmed up to room temperature, and spectra were acquired throughout the heating. We performed in situ transmittance (1–4.35 μm, 10,000–2300 cm^{-1}) or reflectance (1–2.6 μm, 10,000–3800 cm^{-1}) spectroscopy. Further details are given in Appendix A. Spectra were corrected by subtracting baselines to remove interference fringes in the continuum due to the film thickness. We then estimated the 2.27 and 2.34 μm band areas by multi-Gaussian fits.

We corrected the average spectrum of Arrokoth (Grundy et al. 2020) and the spectrum of Pholus (Cruikshank et al. 1998) to remove the spectral continuum. For Pholus, we used a fourth-order polynomial curve to fit the spectrum between 0.44 and 2.42 μm. For Arrokoth, we used the spectrum modeled by Grundy et al. (2020) as a baseline between 2.23 and 2.38 μm. We then calculated the ratio between spectra and baselines. Again, multi-Gaussian fits were used to estimate the areas of methanol bands.

In order to study the effects of surface grain size and different mixtures on the 2.34/2.27 ratio, we also analyzed synthetic spectra of water, methanol and tholins mixtures produced with the Hapke scattering model (Hapke 2012).

3. The 2.34/2.27 μm Band Ratio

Figure 1 shows the Arrokoth (panel (A)) and Pholus (panel (B)) spectra between 2.17 and 2.43 μm and laboratory spectra of ion-processed CH_3OH:H_2O mixtures at 30 and 45 K and after their respective warm-up to 100 K, acquired in transmittance (panels (C) and (D), mixture CH_3OH:H_2O = 5:1) and reflectance (panels (E) and (F), mixture CH_3OH:H_2O = 1:1). We measured the area underneath the 2.27 and 2.34 μm bands to estimate the 2.34/2.27 ratios. The results are shown in Figure 2.

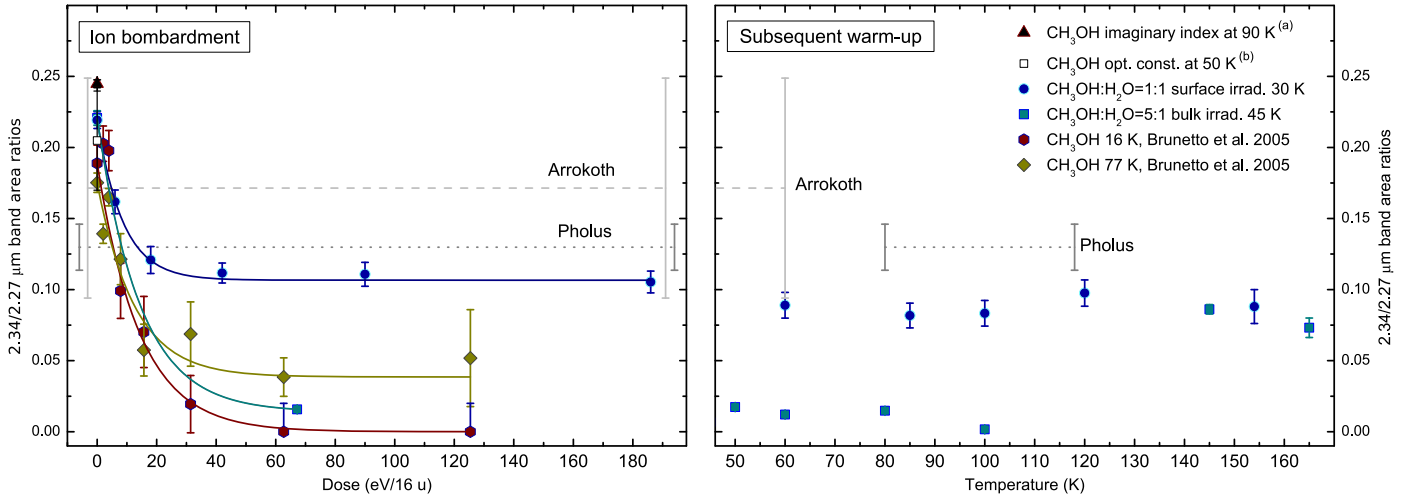

Figure 2. 2.34/2.27 ratios in CH_3OH and CH_3OH:H_2O mixtures exposed to H^+ bombardment (left panel) and subsequent warm-up (right panel). The black triangle and the white square are 2.34/2.27 ratios measured from the optical constants of methanol used by Cruikshank et al. (1998) and Grundy et al. (2020) to model the Pholus and Arrokoth spectra. Solid lines show the fits we performed to calculate the cross section σ. Dashed and dotted lines show the ratios estimated on Arrokoth and Pholus, respectively. In the right panel, the bar length represents the temperature range of the two bodies as given by Stern et al. (2019) and Cruikshank et al. (1998).

3.1. Pholus and Arrokoth

Cruikshank et al. (1998) detected the 2.27 μm band in the Pholus spectrum, while the 2.34 μm band was at the noise level in the spectra reported by Luu et al. (1994). We ran multi-Gaussian fits of the Pholus spectrum to estimate the CH_3OH NIR band areas. We found a single component at 2.27 μm and three components at 2.35, 2.34 and 2.32 μm. We explored various possibilities for the FWHM of the 2.34 μm band. We found two possible solutions for the 2.34/2.27 ratio of 0.159 ± 0.017 and 0.101 ± 0.015, respectively. In Figure 2 we display the 2.34/2.27 ratio as the average, 0.130 ± 0.016.

The spectral sampling of the Arrokoth spectrum is lower than that of the Pholus spectrum. We found a good convergence of only one fit, with two components at 2.27 and 2.34 μm and a 2.34/2.27 ratio of 0.171 ± 0.077. The fits of the Arrokoth and Pholus spectra are shown in Appendix C.

We note that the spectra of Pholus and Arrokoth are averaged spectra obtained from various observations. Therefore, local differences in the 2.34/2.27 ratio could not be detected.

3.2. Laboratory Experiments

The penetration depth of photons into a material depends on their wavelength and on the optical properties of the material. In the NIR, ices exhibit imaginary index $k \sim 10^{-4}$–10^{-2}, and photons can penetrate up to hundreds of micrometers. The penetration depth can be reduced to a few micrometers if a relevant amount of amorphous carbon is present, because it absorbs photons and thus lowers the surface albedo. SW, SEP, and CR have different penetration depths depending on the ion energy and mass (e.g., Strazzulla et al. 2003). To simulate different conditions of ion-processed versus IR-sampled thickness, we performed two experiments: bulk irradiation and surface irradiation. The bulk irradiation experiment simulates high-energy CR and SEP that process the whole NIR-probed thickness. The surface irradiation experiment simulates low-energy ions in the spectra of SEP and SW that penetrate less than NIR photons.

Figures 1(C) and (D) show the transmittance spectra acquired in the bulk irradiation of the CH_3OH:H_2O = 5:1 mixture. We deposited six films of about 700 nm, each of the same composition. Each layer was bombarded with 40 keV H^+ up to 67 eV/16u before the deposition of the subsequent layer.[3] This method allowed us to obtain a fully processed film with a final thickness of 4.2 μm, and an enhanced signal-to-noise ratio in the spectra.

Figure 3 shows the first film before (A) and after irradiation (B). Before EP we estimated a 2.34/2.27 ratio of 0.221 ± 0.005. After EP various new features were found between 2.17 and 2.43 μm. A list of the detected species is provided in Table 1. The 2.34 μm band displayed a strong decrease in intensity and appeared as a shoulder of the CH_4 2.32 μm band, close to the 2.35 μm CO band. As shown in Figure 2, the 2.34/2.27 ratio decreased after EP, remained close to zero up to 100 K during warm-up, and increased between 100 and 145 K. Figure 2 also includes the 2.34/2.27 ratio we estimated from the band areas reported by Brunetto et al. (2005).[4]

In the surface irradiation experiment we used reflectance IR spectroscopy to analyze a 5 μm-thick CH_3OH:H_2O = 1:1 mixture. Ion bombardment was limited to the upper micron of the sample. After deposition at 15 K the mixture was warmed up to 30 K and bombarded with 40 keV H^+ up to 186 eV/16u (Figure 1(E)). After bombardment, we observed a different trend with respect to the bulk irradiation. At ~40 eV/16u a plateau was reached, suggesting that the addition of irradiation only affected the already-processed surface, while the underlying methanol remained unaltered. During warm-up to 100 K, the ratio lowered slightly at 60 K and then remained constant up to the sample sublimation. Through the multi-Gaussian fit procedure, we found contributions of CH_4 at 2.33 μm and CO at 2.35 μm. Additional details are given in Appendix A.

[3] According to calculations with the SRIM software (Ziegler et al. 2008), assuming a mixture density of 0.8 g cm^{-3}, the penetration depth of the 40 keV H^+ beam is ~1.1 μm. Up to 700 nm ion implantation is negligible.

[4] Note that Brunetto et al. (2005) gave the normalized band area values. In order to calculate the 2.34/2.27 ratio we used nonnormalized values provided by the authors.

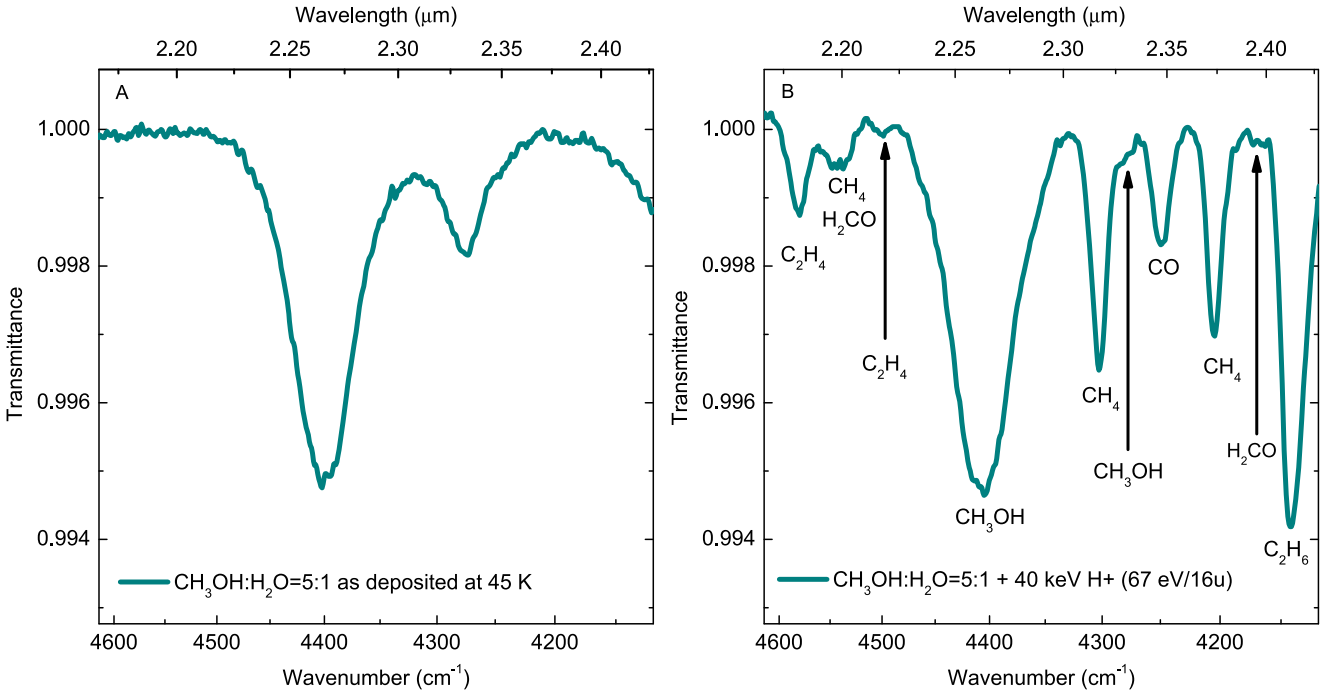

Figure 3. Comparison between the spectra of $CH_3OH:H_2O = 5{:}1$ mixture before (panel (A)) and after irradiation with 40 keV H^+ at 45 K (panel (B)). Labels indicate the compounds responsible for the absorptions.

The 2.34/2.27 ratios in Figure 2 were fitted with the exponential function $y = y_0(\alpha \exp(-\sigma D) + 1 - \alpha)$, where y_0 is the ratio before irradiation, $0 < \alpha \leqslant 1$ is a parameter that affects the value of the asymptote, σ is the cross section of the process in 16u/eV, and D is the dose in eV/16u. The cross section and the values of α are listed in Table B1 in Appendix B. The function was fit to the data collected in the various experiments by varying σ and α. The cross section is derived from the combination of the destruction cross sections of the 2.34 μm and of the 2.27 μm bands, in which the latter has a lower value from being less sensitive to irradiation. The values of α are related to the ratio between the processed thickness and the IR-probed thickness: the higher the ratio, the lower the asymptote.

4. Discussion

The higher sensitivity of the 2.34 μm band with respect to the 2.27 μm band to ion bombardment was represented in our experiments as a decrease of 2.34/2.27 ratios with increasing dose. In the bulk irradiation, the ratio was determined to be ~zero at about 67 eV/16u because at this dose the 2.34 μm band was almost completely destroyed. Further experiments on a $CH_3OH:H_2O = 3{:}1$ mixture bombarded with 40 keV H^+ at 15 K showed that about 90% of the initial methanol was destroyed after a similar irradiation dose (85 eV/16u). Even if the destruction cross section of the 2.34 μm band was found to be higher than that of the 2.27 μm band, at high dose the destruction of the 2.27 μm band was not negligible and the exponential decaying behavior of the 2.34/2.27 ratio observed at lower doses was lost. In the surface irradiation experiment, we observed a decrease in the 2.34/2.27 ratio, and a plateau from 20 to 40 eV/16u because of unprocessed methanol beneath the irradiated surface. Variation in the 2.34/2.27 ratio observed during warm-up in the bulk irradiation experiment (see the right panel of Figure 2) could be attributed to methanol and water phase changes between 100–140 K and 150–160 K (e.g., Palumbo et al. 1999), respectively, that affect the band strengths.

To test the effects of particle size and mixture ratio on the 2.34/2.27 ratios, we used the Hapke model (Hapke 2012) to produce synthetic spectra of regolith surfaces rich in water and methanol, varying the relative abundances and grain size, and also including tholins. In none of the simulated cases were we able to reproduce the 2.34/2.27 ratios found after irradiation of methanol-rich samples. Thus, the variations we observed in the experiments can only be attributed to EP. Additional details are provided in Appendix D.

4.1. Timescales of Processing

Estimation of the 2.34/2.27 ratio could provide constraints on the exposure timescales of methanol-rich surfaces to EP at typical temperatures for KBOs. The 2.34/2.27 ratio decreased significantly after an irradiation dose of about 40 eV/16u. We estimated the time necessary for a methanol-rich surface to accumulate such a dose by CR, SW, and SEP bombardment.

CR mainly consists of protons (87%) and helium (12%) ions, with heavier ions accounting for the remaining ~1%. Their energy spans between a few keV and 10^{18} keV (e.g., Johnson 1990; Rothard et al. 2017). According to Strazzulla et al. (2003), a 10 μm-thick surface at 40 au would accumulate 100 eV/16u in about 8×10^9 yr. At the current orbit of Arrokoth (semimajor axis 44.63 au), 40 eV/16u would have accumulated in 3–4 $\times$ 10^9 yr.

SW is a supersonic flux of ions and electrons coming from the solar corona with energies ~1 keV/u. SW flux decreases with the square of distance from the Sun, and H^+ are the main components (~96%). Near Arrokoth, the SWAP instrument on board New Horizons measured an SW flux of 8.5×10^4 H^+ cm^{-2} s^{-1} (Stern et al. 2019). 40 eV/16u corresponds to a fluence of 3.4×10^{15} H^+ cm^{-2}. When we divide the

Table 1
Near-infrared Bands between 2.18 and 2.41 μm in Irradiated $C_3OH:H_2O = 5:1$

Band position (μm)	(cm^{-1})	Vibrational mode	Attribution	Reference
2.183	4580	$\nu_{11} + \nu_2$ C–H	C_2H_4	Abplanalp & Kaiser (2017)
2.201	4543	$\nu_2 + \nu_3$ C–H	CH_4	Quirico & Schmitt (1997)
		ν C=O+C–H	H_2CO	This work[a]
2.223	4499	$\nu_5 + \nu_{12}$ C–H	C_2H_4	Abplanalp & Kaiser (2017)
2.269	4407	ν_a+def. C–H	CH_3OH	Cruikshank et al. (1998)
2.324	4303	$\nu_3 + \nu_4$ C–H	CH_4	Quirico & Schmitt (1997)
2.336	4280	ν_s+def C–H.	CH_3OH	Cruikshank et al. (1998)
2.354	4248	$2\nu_2$ CO	CO	Gerakines et al. (2005)
2.379	4204	$\nu_1 + \nu_4$ C–H	CH_4	Quirico & Schmitt (1997)
2.396	4172	ν C=O + C–H	H_2CO	This work[a]
2.414	4142	ν+def. C–H	C_2H_6	Quirico & Schmitt (1997)

Note.
[a] Tentative assignments based on the mid-IR H_2CO bands reported by Schutte et al. (1993). Abplanalp & Kaiser (2017) reported a C_2H_4 band at 2.186μm. Quirico & Schmitt (1997) reported a CH_4 band at 2.208μm. Quirico & Schmitt (1997) reported a 2.41μm band for 1% C_2H_6 in N2.

fluence by the H^+ flux measured by SWAP, we obtain the timescale to accumulate such a dose on Arrokoth, i.e., about 1.3×10^3 yr. However, SW protons only affect the upper $\sim$100 nm of an icy surface,[5] $\leqslant$10% than the IR-sampled thickness (IR photons penetrate between 1 and hundreds of μm), thus observations with a very high signal-to-noise would be required to detect their effect.

Active solar regions and flares emit SEP. H^+ are the main components (95%) and the flux decreases as for SW ions, but their energy is much higher, tens of keV—hundreds of MeV. Mewaldt et al. (2007) reported fluence spectra for protons over a period of 8.25 yr. The lower energy protons ($\sim$50 keV) show a fluence of about 2×10^{12} cm^{-2}, with a flux of 7.7×10^3 H^+ cm^{-2} s^{-1}. At the orbit of Arrokoth, the SEP flux corresponds to 3.86 H^+ cm^{-2} s^{-1}, thus 40 eV/16u would have accumulated in $\sim 3 \times 10^7$ yr. At the current orbit of Pholus (semimajor axis 20.39 au), the SEP flux is approximately 5 times higher than the flux at the orbit of Arrokoth, $\sim$19 H^+ cm^{-2} s^{-1}. To accumulate 40 eV/16u would require $\sim 6 \times 10^6$ yr. Even with a lower fluence, between 10^{11} and 10^6 H^+ cm^{-2}, more energetic particles contribute to the process, reducing the time necessary to accumulate 40 eV/16u. These estimates suggest the primary role of SEP in the EP of atmosphere-less icy surfaces in the outer solar system, with timescales that are much lower than that required for CR processing. Taking into account that Brunetto et al. (2006) observed the reddening of processed-methanol ice after a dose of 44 eV/16u, SEP could account for the red slopes observed on both Pholus and Arrokoth.

4.2. A Spectroscopic Probe of Irradiation

We analyzed the NIR methanol bands in Arrokoth and Pholus spectra, and we tested the 2.34/2.27 ratio as a spectroscopic probe of EP of methanol-rich surfaces. Figure 2 shows that the 2.34/2.27 ratio on Pholus is close to the typical values of a processed ice, while Arrokoth shows a ratio close to that observed in unprocessed or low-processed methanol-rich ice. However, error bars hindered a precise estimation of the absorbed dose.

Figure 4 shows the penetration depth of energetic particles and IR-photons on surfaces. CR penetrate up to tens of meters deep, but because of the low energy loss (0.02–0.35 eV/Å) they require billions of years to affect the 2.34/2.27 ratio. In contrast, SEP can penetrate micrometers to centimeters, have high energy loss (0.35–8 eV/Å), and can lower the ratio in about 10^6–10^7 yr. The value of the 2.34/2.27 ratio asymptote α depends on the ratio between IR-sampled and processed thickness. NIR photons penetrate a few to hundreds of micrometers, according to the imaginary index k that is found to be about $\sim 10^{-4}$–10^{-2} for frozen volatiles and that can be significantly increased to $\sim 10^{-1}$ if amorphous carbon is present. If $k \sim 10^{-1}$ (case 1 in Figure 4), and due to the fast timescale of EP by SEP with respect to the age of KBOs, we would expect a 2.34/2.27 ratio close to zero. The whole IR-sampled thickness would be processed, as in the bulk irradiation experiment. If $k \sim 10^{-4}$–10^{-2} (case 2 in Figure 4), IR-photons penetrate hundreds of micrometers, a greater depth than SEP, thus unprocessed methanol would be probed. This would prevent detection of 2.34/2.27 ratios close to zero, as we observed in our surface irradiation study.

Rejuvenating processes could expose fresh subsurface material, resulting in an increase in the ratio. However, the Arrokoth surface dates to the end of the solar system accretion (Spencer et al. 2020) and has not been altered by rejuvenating processes, thus we suggest that remote sensing probed a larger thickness than the SEP penetration depth, and unprocessed methanol produced the high ratio we estimated. We do not exclude, however, the possible migration of buried volatiles toward the surface, as observed on Eris and Pluto surfaces (e.g., Bertrand et al. 2019; Hofgartner et al. 2019, and references therein). If such a process occurs on localized portions of surface, the estimation of 2.34/2.27 ratio may distinguish between recently exposed and old regions.

4.3. Further Evidence of EP

Together with methanol bands, the fit of the Pholus spectrum revealed features at 2.32 and 2.35 μm (see Appendix C). At these wavelengths, we observed CH_4 and CO bands in the bulk irradiation experiment (Figure 1 panel (C)), still present at 100 K. In Figure B1 we overlap and compare the Pholus and the laboratory spectra. The signal-to-noise ratio is too low for a 3σ detection of CH_4 and CO; however, the comparison suggested the presence of both compounds on the centaur, and experimental results showed they formed due to EP of the

[5] As found in SRIM simulations for 1 keV H^+ on a $CH_3OH:H_2O = 5:1$ ice with a density of 0.8 g cm^{-3}.

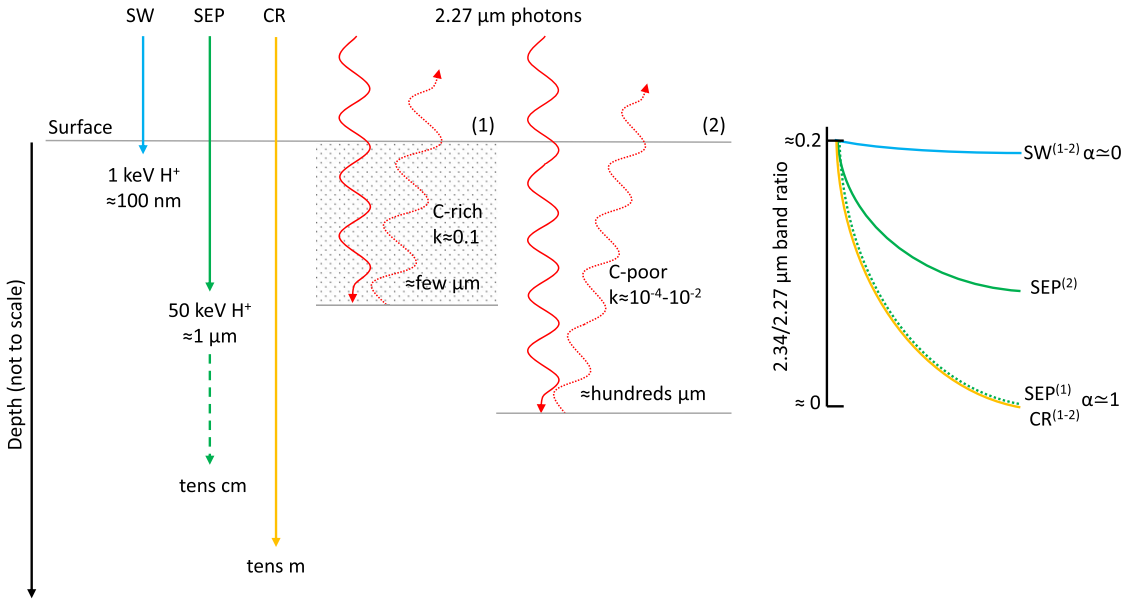

Figure 4. Penetration depths of SW, SEP, and CR. For SW and SEP we show 1 keV H^+ and 50 keV H^+, respectively, the main populations in terms of energy and flux. Red arrows represent incident (solid) and reflected (dotted) 2.27 μm photons on a surface rich in amorphous carbon (C-rich) or rich in frozen volatiles (C-poor). The right part of the figure shows expected 2.34/2.27 ratios after irradiation by SW, SEP, and CR according to the IR-sampled thickness and the expected values of α.

methanol-rich surface. Furthermore, a feature at 2.41 μm that could be attributed to C_2H_6 seems to be present on the Arrokoth small lobe (Grundy et al. 2020). Grundy et al. (2020) suggested that on Arrokoth, EP of CH_4 and H_2O was at the origin of CH_3OH as well as C_2H_4 and C_2H_6, precursors of tholins. However, neither CH_4 nor H_2O were detected and as we have shown, the synthesis of both C_2H_4 and C_2H_6 as well as C-rich refractory material could be explained by EP of methanol-rich mixtures. Furthermore, in the ISM, methanol was detected with abundances as high as ∼30% with respect to water, while methane was between 0.4% and 11% (e.g., Boogert et al. 2015). Thus, methanol could be a pristine compound accreted in KBOs during their formation.

Our results suggest that post-accretional EP by SEP could account for the vis-NIR slopes of Arrokoth and Pholus. However, the red color could be also due to accretion of red matter present in the protoplanetary disk during the planetesimals formation, possibly inherited from presolar grains (e.g., Strazzulla et al. 2003). Molecules containing chromophores could have been present in the disk and remained trapped during the accretion of planetesimals. Also in this case, EP could have played a fundamental role in the synthesis of chromophore species due to the interaction between CR and icy grain mantles, a process that may explain the presence of organics in meteorites (e.g., Nakamura-Messenger et al. 2006), suggesting that icy grain mantles were already processed before the accretion in primitive bodies (e.g., Dalle Ore et al. 2011).

5. Conclusions

Methanol was detected on the KBO Arrokoth and the centaur Pholus. In the future, methanol could be revealed on other KBOs, thanks to the extension of the New Horizons mission and to observations performed with new generation instruments. The Near InfraRed Spectrograph (NIRSpec) on board the James Webb Space Telescope will allow observations between 0.6 and 5.3 μm, with a much higher sensitivity than that of currently available instruments, and could lead to identification of methanol-rich surfaces.

The experiments we performed simulated the EP of methanol-rich objects. We showed that the 2.34/2.27 μm methanol band ratio is sensitive to ion bombardment, and we determined that SEP are the primary contributors in inducing changes in the NIR spectra of icy surfaces in the outer solar system. Estimating the 2.34/2.27 μm band ratio could allow the differentiation between objects that were exposed to different levels of irradiation, to identify less altered regions on the same object, and to obtain timescales for the exposure of a surface, independently from vis-NIR slopes.

We thank the reviewers for their helpful comments. We thank O. Mivumbi for the support during experiments, as well as D. Ledu and C.O. Bacri for the access to the SIDONIE facility. INGMAR is a IAS-CSNSM facility funded by the French Programme National de Planétologie (PNP), Faculté des Sciences d'Orsay, Université Paris-Sud (Attractivité 2012), French National Research Agency ANR (contract ANR-11-BS56-0026, OGRESSE), P2IO LabEx (ANR-10-LABX-0038) in the framework Investissements d'Avenir (ANR-11-IDEX-0003-01). We thank the support from RAHIIA SSOM (ANR-16-CE29-0015). We thank A. Arondel, P. Duret, S. Blivert, and M. Godard for their contribution in the realization of INGMAR, G. Strazzulla, G.A. Baratta, M.E. Palumbo, C. Lantz and L. d'Hendecourt for fruitful discussions. We thank S. Seto for the language editing. N.P.-A. acknowledges funding support from SRI/FSI through the project "Finding the recipe to cook a primitive small body in the Solar System." R.G.U. thanks the CNES postdoctoral program.

Appendix A
Experimental Methods

Water and methanol vapor mixtures were prepared in a mixing chamber ($P \leqslant 10^{-4}$ mbar). Through a needle valve, mixtures were then injected in the main vacuum chamber ($P \sim 5 \times 10^{-8}$ mbar) that hosted a substrate in thermal contact with the cold finger of a closed-cycle He cryocooler (CTI, 14–300 K). Preliminary experiments were performed to calibrate the substrate temperature by depositing pure water at 15 K and warming up to the temperature of water crystallization. In the IR spectra we examined the position of water bands during warm-up, and they were found to correspond within error bars with the band positions reported by Mastrapa et al. (2009). We performed further depositions at 15 K with water and methanol mixtures and we estimated a deposition rate of $\sim$50 nm min^{-1}. In the experiments reported here depositions were performed at 15 K for the surface irradiation experiment and 45 K for the bulk irradiation experiment. In the surface irradiation experiment we wanted to obtain a thick ice (about 5 μm), thus we kept the substrate temperature at 15 K to speed up the deposition (faster at lower temperature). We then warmed up the sample to 30 K at the end of the deposition, before starting the ion bombardment. We verified that for the goal of this work (studying the 2.34/2.27 μm band ratio) the different deposition temperatures do not have any influence on the results. In the bulk irradiation experiment we deposited six layers of about 700 nm each at 45 K and ion bombardment was performed between each deposition step at the same temperature. We verified that the two preparation conditions are equivalent in terms of 2.34/2.27 μm band ratio. In the bulk irradiation experiment, a 5 cm-long copper tube was placed on the back of the sample holder to hinder the deposition of the mixture on the backside of the substrate.

Samples were analyzed in situ by means of a Fourier-Transform infrared spectrometer (Bruker Tensor). Mirrors on an optical bench guided the IR beam to the vacuum chamber, and the beam entered it through a ZnSe window. In transmittance mode, the incident beam arrived on the sample with an angle of 10° with respect to the surface normal and was then collected by an MCT detector placed on the other side of the vacuum chamber. Reflectance spectra were obtained with the same illumination geometry, while reflected diffuse light was collected by an NIR optical fiber placed at 10° with respect to the surface normal but on a different plane (phase angle 14°.1). Sample thickness was estimated a priori with the deposition rate and we then determined the final thickness by examining the position of minima and maxima in the interference pattern of the NIR spectral continuum.

This method required the refractive index n of the deposited film. We averaged the values of n for pure water (1.31) and pure methanol (1.33, e.g., Scirè et al. 2019) according to the mixtures ratio. We estimated an error $\leqslant$20% on the final thickness. IR spectra were collected with a resolution of 1 cm^{-1} in transmittance mode and 2 cm^{-1} in reflectance mode.

Samples were bombarded with 40 keV H^+ produced by the SIDONIE ion accelerator (CSNSM, Orsay). The ion beam arrived on samples at an angle of 10° with respect to the surface normal. The ion beam was rastered in order to ensure a homogeneous covering of the sample surfaces. To measure the ion current, a brass ring placed before the entrance of the vacuum chamber was used. The brass ring and the inner hole areas were known, so we estimated the number of ions that passed through the ring by measuring the number of ions that hit the ring. Preliminary calibration experiments were performed using a Faraday cup installed inside the vacuum chamber, in order to measure the fluence that arrived on the samples. During ion bombardment, in real time, we integrated the ion current to estimate the fluence (ions cm^{-2}). We then multiplied the fluence by the stopping power in eV cm^2/16u calculated with the SRIM software (Ziegler et al. 2008) and we obtained the dose in eV/16u (e.g., Strazzulla & Johnson 1991). To avoid the macroscopic heating of the sample, we used ion current densities lower than 800 nA cm^{-2}.

In Figure 2 we added data obtained by Brunetto et al. (2005). In their work, reflectance spectra were acquired on pure methanol deposited at 16 and 77 K up to a final thickness of 1 μm and bombarded with 200 keV H^+. For this ion energy, the H^+ penetration depth was about 2 μm, i.e., higher than the ice thickness. We calculated the irradiation doses by multiplying the fluences given in Brunetto et al. (2005) by the stopping power in eV cm^2/16u obtained through the SRIM software for a 1 μm-thick CH_3OH sample with a density of 0.8 g cm^{-3} bombarded with 200 keV H^+.

Appendix B
Ion-induced Synthesis in Frozen Water and Methanol Mixtures

In the spectra in Figures 1 and 3 acquired in the bulk irradiation experiment, we identified various vibrational bands that were due to the formation of new compounds in the methanol-rich sample. In fact, the impinging ions released their energy to the target along their path, inducing the break of chemical bonds. Radicals and molecular fragments then recombined to form new compounds (e.g., Rothard et al. 2017). We identified bands attributed to CH_4, C_2H_4, C_2H_6, and CO. We also identified two bands at 2.201 and 2.396 μm that we tentatively assigned to H_2CO. Schutte et al. (1993) reported the vibrational bands of pure H_2CO in the mid-IR. Combining the C = O stretching modes at 1177 and 1723 cm^{-1} with the C–H stretching modes at 2991 and 2822 cm^{-1} we obtained combination modes at 4168 cm^{-1} (2.399 μm) and 4545 cm^{-1} (2.200 μm), respectively. The slight shifts in the band positions we observed could be attributed to the dilution of H_2CO in the frozen matrix. The 2.201 μm band could be also attributed to CH_4, as reported by Quirico & Schmitt (1997). We note that additional features were found at longer wavelengths. In particular, an intense band at 4.27 μm attributed to CO_2, an abundant by-product of methanol processing (e.g., Bennett & Kaiser 2007). Because of sublimation, bands attributed to newly synthesized species decreased during the sample warm-up. In particular, the CH_4 band disappeared at 145 K, while the CO feature was still detected up to 165 K, even if very low in intensity. Pure CO and CH_4 sublimate at temperatures lower than 40 K, but their presence at these relatively high temperatures was due to trapping in the methanol-water matrix (e.g., Collings et al. 2004).

In the surface irradiation experiment, we were able to fit the 2.34 μm band with three components, centered at 2.33, 2.34, and 4.35 μm, attributed to CH_4, CH_3OH, and CO, respectively. From data fitting, we found the 2.34 μm CH_3OH band up to

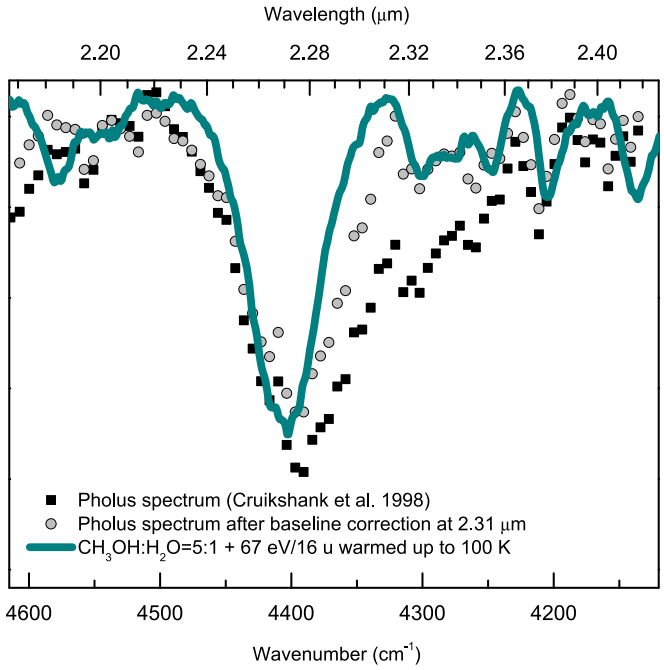

Figure B1. The spectrum of Pholus after the correction at 2.31 μm shows a better overlap with the transmittance laboratory spectra acquired on the CH_3OH:H_2O = 5:1 mixture after ion bombardment and warm-up to 100 K.

Table B1
Cross Sections

Mixture	Temperature (K)	Initial ratio y_0	α	σ (16 u/eV)
CH_3OH[a]	15	0.189	1.00	0.07 ± 0.02
CH_3OH[a]	77	0.175	0.78	0.08 ± 0.02
CH_3OH:H_2O=1:1[b]	30	0.219	0.51	0.12 ± 0.03
CH_3OH:H_2O=5:1[b]	45	0.221	0.94	0.07 ± 0.03

Notes. Mixture, temperature of irradiation, initial 2.34/2.27 ratio at dose zero (y_0), $0 < \alpha \leqslant 1$ affects the value of the asymptote, σ is the cross section in 16u/eV and D is the dose in eV/16 u. When $\alpha \simeq 0$, the asymptote corresponds to y_0. When $\alpha = 1$, the asymptote tends to 0.
[a] Experiments reported by Brunetto et al. (2005).
[b] This work.

180 K. CH_4 is found up to 100 K, while CO is found up to 120 K. The contribution of these features was not as evident as in the bulk irradiation experiment. This could be explained by (i) the higher dilution of methanol in water (1:1) with respect to the bulk irradiation experiment (5:1) that determined a lower efficiency in the by-products synthesis; (ii) the IR-sampled thickness was higher than the ion beam penetration depth, thus the relative abundance of CO and CH_4 was too low to be detected in this configuration.

As reported in Section 3.2 we estimated the cross section σ for the 2.34/2.27 ratio with increasing irradiation dose. In Table B1 we list the mixture ratios, temperature at which bombardment was performed, the initial 2.34/2.27 ratios, the value of α and the cross section σ.

In Figure B1 we show the Pholus spectrum after the baseline correction at 2.31 μm, the same method we used to correct laboratory spectra of CH_3OH:H_2O mixtures acquired at 100 K after ion bombardment. The comparison between the observed spectrum of Pholus and the transmittance laboratory spectrum helps display the similarities, even if shifts of $\sim$10 cm^{-1} in the peak position are present.

Appendix C
Gaussian Fits of Pholus and Arrokoth Spectra

The Arrokoth and Pholus spectra reported by Grundy et al. (2020) and Cruikshank et al. (1998), respectively, were first corrected to remove baselines, as reported in Section 3.1. We

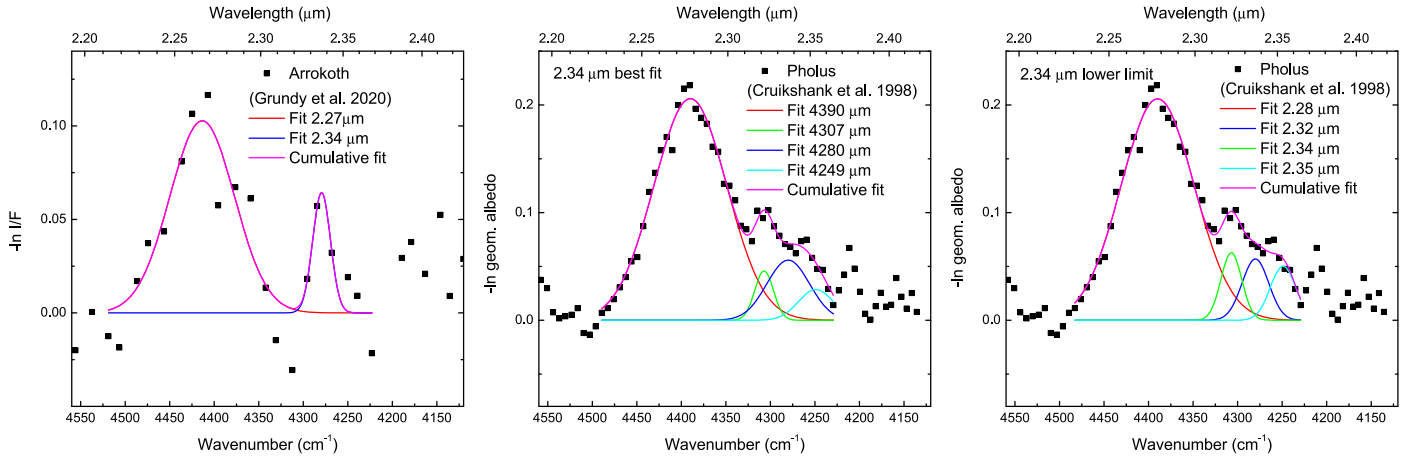

Figure C1. Fits of the spectra of Arrokoth and Pholus in the range of 2.20–2.22 μm. For Pholus we show the best fit of the spectrum (central panel) and the fit with the lowest value of the 2.34 μm band area we found by reducing the band FWHM (right panel).

then calculated the natural logarithm of the intensity scales of spectra (given in *I/F* for Arrokoth and in *Geometric Albedo* for Pholus) to run the multi-Gaussian fit procedure. The Arrokoth spectrum was fitted with two components centered at 2.27 and 2.34 μm. For Pholus, we used four Gaussian curves centered at 2.27, 2.35, 2.34, and 2.32 μm, the same number of components and the same positions we identified in laboratory spectra of the bulk irradiation experiment. The fits are shown in Figure C1.

Appendix D
Modeling of Methanol-rich Surfaces

The Hapke theory (Hapke 2012) was first proposed in 1981 to compute the reflectance spectrum of regolith surfaces where the grain size is larger than the incident wavelength. Using the Hapke model it is possible to compute the reflectance of a surface and obtain information on its composition. By means of the Hapke model, Cruikshank et al. (1998) computed the abundances of water, methanol, and other components on the Pholus surface. Information on surface composition can be obtained also with the Shkuratov theory (Shkuratov et al. 1999). This model was used by Poulet et al. (2002) to reanalyze the Pholus spectrum. Poulet et al. (2002) compared the results obtained by means of the Hapke and Shkuratov models, and even though they identified the same components reported by Cruikshank et al. (1998), relative abundances were different. According to the authors, these discrepancies are due to the different scattering theories employed.

We used the Hapke model (Hapke 2012) to simulate spectra of a surface with intimate mixtures of water and methanol grains in various relative abundances, with or without tholins. Spectra A, B, and C in Figure D1 are from mixtures with 50% water particles of 30 μm and 50% methanol particles of 10, 30, and 100 μm, respectively. Spectra D and C are from mixtures with water, methanol, and Titan tholins particles of 30 μm each. Figure D1 also shows the spectrum of Pholus as modeled by Cruikshank et al. (1998). Their model included grains of water, methanol, olivine, Titan tholins and carbon black, and it showed a 2.34/2.27 ratio of 0.299 ± 0.027. In the synthetic spectra we estimated 2.34/2.27 ratios that were always $\geqslant$0.34. We were not able to reproduce the low ratio observed after the ion bombardment of methanol-rich ices.

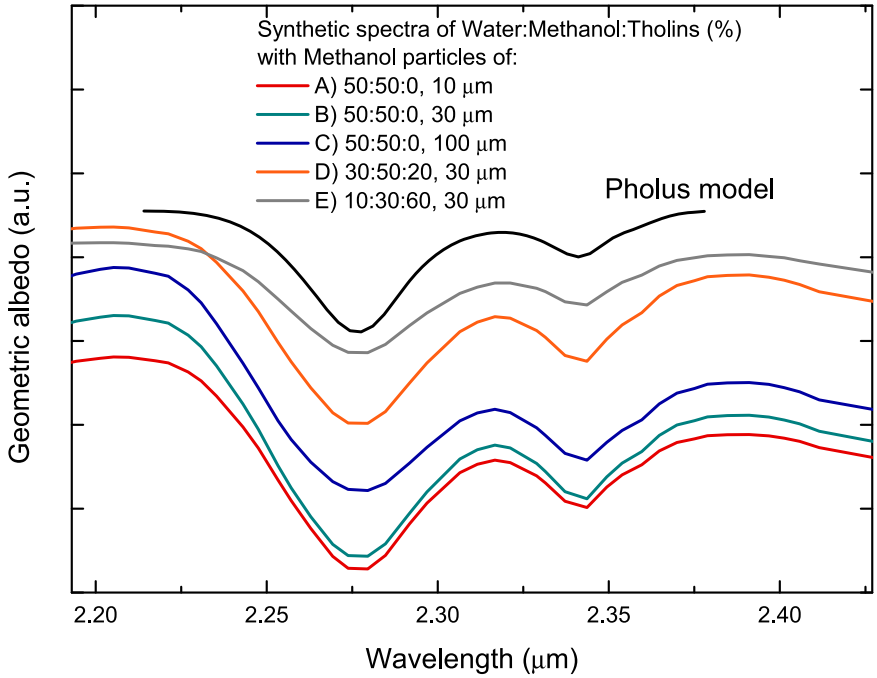

Figure D1. Synthetic spectra in the range 2.2–2.4 μm produced with the Hapke model of mixtures of water and methanol particles with the following abundances: (A) 50% each, methanol particles of 10 μm; (B) 50% each, methanol particles of 30 μm; (C) 50% each, methanol particles of 100 μm; (D) 30% water, 50% methanol and 20% Titan Tholins, methanol particles of 30 μm; (E) 10% water, 30% methanol and 60% Titan Tholins, methanol particles of 30 μm. In all cases, water and Titan tholins grains had 30 μm size.

Appendix E
The Penetration Depths of Energetic Particles and IR Photons

In Figure 4 we show a schematic representation of the penetration depths of SW ions, SEP, and CR in atmosphere-less surfaces. For SW and SEP, H^+ at 1 keV and 50 keV, respectively, are the main ion populations in terms of flux and energy (Johnson et al. 1987; Mewaldt et al. 2007). H^+ are also the main population in CR. They have a wide energy spectrum (up to 10^{18} keV), thus they can penetrate deeper, up to tens of meters deep. However, they have low energy loss with respect to low-energy particles in the SEP spectrum. Thus, to affect the physico-chemical properties of frozen surfaces, CR require much larger timescales (3–4 billion years) with respect to SEP (10^6–10^7 yr). The red arrows denote the penetration depth of 2.27 μm photons in two limit cases, (1) low penetration, up to a few micrometers, on a surface where frozen volatiles are mixed with a large amount of amorphous carbon (~60%) that is responsible for an imaginary index $k \sim 0.1$–0.2 at 2.27 μm; (2) high penetration, up to hundreds of μm, on a surface dominated by frozen volatiles with low absorption and an imaginary index $k \sim 10^{-4}$–10^{-2} at 2.27 μm. In case (1), SEP (green arrow) and CR (yellow arrow) process the whole IR-sampled thickness and beyond. IR photons probe a layer where methanol was affected by irradiation and the 2.34/2.27 ratio would be ~0. SW ions (blue arrow) implant within ~100 nm, thus with a limited alteration with respect to the IR-sampled thickness. In case (2), because of the low value of k, IR photons can penetrate up to hundreds of micrometers. Thus, CR process the whole IR-sampled thickness, the low penetration of SW ions determines that they would affect the ratio even less than in case (1), and SEP implant within the IR-sampled thickness. As a result, IR photons probe both processed and unprocessed methanol. The 2.34/2.27 ratio will depend on the ratio between the SEP-processed and IR-sampled thickness, as we have seen in the surface irradiation experiment, where we found an asymptotic value $\alpha < 1$.

ORCID iDs

Riccardo Giovanni Urso https://orcid.org/0000-0001-6926-1434
Donia Baklouti https://orcid.org/0000-0002-2754-7829

References

Abplanalp, M. J., & Kaiser, R. I. 2017, ApJ, 836, 195
Allamandola, L. J., Sandford, S. A., & Valero, G. J. 1988, Icar, 76, 225
Altwegg, K., Balsiger, H., Berthelier, J. J., et al. 2017, MNRAS, 469, S130
Barucci, M. A., Merlin, F., Dotto, E., Doressoundiram, A., & de Bergh, C. 2006, A&A, 455, 725
Bennett, C. J., Chen, S.-H., Sun, B.-J., Chang, A. H. H., & Kaiser, R. I. 2007, ApJ, 660, 1588
Bennett, C. J., & Kaiser, R. I. 2007, ApJ, 661, 899
Bertrand, T., Forget, F., Umurhan, O. M., et al. 2019, Icar, 329, 148
Boogert, A. C. A., Gerakines, P. A., & Whittet, D. C. B. 2015, ARA&A, 53, 541
Brunetto, R., Baratta, G. A., Domingo, M., & Strazzulla, G. 2005, Icar, 175, 226
Brunetto, R., Barucci, M. A., Dotto, E., & Strazzulla, G. 2006, ApJ, 644, 646
Chauvin, N., Dayras, F., Le Du, D., & Meunier, R. 2004, NIMPR, 521, 149
Chen, Y. J., Ciaravella, A., Muñoz Caro, G. M., et al. 2013, ApJ, 778, 162
Chuang, K. J., Fedoseev, G., Qasim, D., et al. 2017, MNRAS, 467, 2552
Collings, M. P., Anderson, M. A., Chen, R., et al. 2004, MNRAS, 354, 1133
Cruikshank, D. P., Roush, T. L., Bartholomew, M. J., et al. 1998, Icar, 135, 389
Dalle Ore, C. M., Fulchignoni, M., Cruikshank, D. P., et al. 2011, A&A, 533, A98
de Barros, A. L. F., Bordalo, V., Seperuelo Duarte, E., et al. 2011, A&A, 531, A160
Eberhardt, P., Meier, R., Krankowsky, D., & Hodges, R. R. 1994, A&A, 288, 315
Geiss, J., Altwegg, K., Anders, E., et al. 1991, A&A, 247, 226
Gerakines, P. A., Bray, J. J., Davis, A., & Richey, C. R. 2005, ApJ, 620, 1140
Gerakines, P. A., Schutte, W. A., & Ehrenfreund, P. 1996, A&A, 312, 289

Grundy, W., Bird, M., Britt, D., et al. 2020, Sci, 367, aay3705
Hapke, B. 2012, Theory of Reflectance and Emittance Spectroscopy (2nd ed.; Cambridge: Cambridge Univ. Press)
Hofgartner, J. D., Buratti, B. J., Hayne, P. O., & Young, L. A. 2019, Icar, 334, 52
Hudson, R. L., & Moore, M. H. 2000, Icar, 145, 661
Johnson, R. E. 1990, Energetic Charged-particle Interactions with Atmospheres and Surfaces (Berlin: Springer)
Johnson, R. E., Cooper, J. F., Lanzerotti, L. J., & Strazzulla, G. 1987, A&A, 187, 889
Lantz, C., Brunetto, R., Barucci, M. A., et al. 2017, Icar, 285, 43
Luu, J., Jewitt, D., & Cloutis, E. 1994, Icar, 109, 133
Mastrapa, R. M., Sandford, S. A., Roush, T. L., Cruikshank, D. P., & Dalle Ore, C. M. 2009, ApJ, 701, 1347
McKinnon, W., Richardson, D., Marohnic, J. C., et al. 2020, Sci, 367, aay6620
Mewaldt, R. A., Cohen, C. M. S., Mason, G. M., Haggerty, D. K., & Desai, M. I. 2007, SSRv, 130, 323
Modica, P., Palumbo, M. E., & Strazzulla, G. 2012, P&SS, 73, 425
Nakamura-Messenger, K., Messenger, S., Keller, L. P., Clemett, S. J., & Zolensky, M. E. 2006, Sci, 314, 1439
Nesvorný, D. 2018, ARA&A, 56, 137
Nuevo, M., Cooper, G., & Sandford, S. A. 2018, NatCo, 9, 5276
Palumbo, M. E., Castorina, A. C., & Strazzulla, G. 1999, A&A, 342, 551
Poston, M. J., Mahjoub, A., Ehlmann, B. L., et al. 2018, ApJ, 856, 124
Poulet, F., Cuzzi, J. N., Cruikshank, D. P., Roush, T., & Dalle Ore, C. M. 2002, Icar, 160, 313
Quirico, E., & Schmitt, B. 1997, Icar, 127, 354
Rothard, H., Domaracka, A., Boduch, P., et al. 2017, JPhB, 50, 062011
Schutte, W. A., Allamandola, L. J., & Sandford, S. A. 1993, Icar, 104, 118
Scirè, C., Urso, R. G., Fulvio, D., Baratta, G. A., & Palumbo, M. E. 2019, AcSpA, 219, 288
Shkuratov, Y., Starukhina, L., Hoffmann, H., & Arnold, G. 1999, Icar, 137, 235
Souza-Feliciano, A. C., Alvarez-Candal, A., & Jiménez-Teja, Y. 2018, A&A, 614, A92
Spencer, J., Stern, S., Moore, J., et al. 2020, Sci, 367, aay39999
Stern, S. A., Weaver, H. A., Spencer, J. R., et al. 2019, Sci, 364, aaw9771
Strazzulla, G., Cooper, J. F., Christian, E. R., & Johnson, R. E. 2003, CRPhy, 4, 791
Strazzulla, G., & Johnson, R. E. 1991, in Comets in the Post-Halley Era, Vol. 1, ed. R. L. Newburn, Jr. et al. (Dordrecht: Kluwer), 243
Ziegler, J. F., Biersack, J. P., & Ziegler, M. D. 2008, NIMPB, 268, 1818